Food Chemistry 327 (2020) 127047

Contents lists available at ScienceDirect

Food Chemistry

journal homepage: www.elsevier.com/locate/foodchem

The analysis of the effects of high hydrostatic pressure (HHP) on amylose molecular conformation at atomic level based on molecular dynamics simulation

Chen Zhi-guang[a,b], Zhang Hong-hui[a,1], Wade Keipper[c], Pu Hua-yin[a], Yang Qi[a], Fang Chen-lu[a], Shu Guo-wei[a], Huang Jun-rong[a,*]

[a] Shaanxi University of Science and Technology, School of Food and Biological Engineering, Xi'an, Shaanxi Province 710021, China
[b] Neijiang Vocational and Technical College, Department of Agricultural Technology, Neijiang, Sichuan Province 641000, China
[c] Shaanxi University of Science and Technology, School of Arts and Sciences, Xi'an, Shaanxi Province 710021, China

ARTICLE INFO

Keywords:
Molecular dynamics simulation
HHP
Amylose
Molecular conformation

ABSTRACT

For more effective using of HHP (high hydrostatic pressure) in starch processing, in this study, molecular dynamics simulation was used to explore the effects of pressure on amylose molecular conformation at the atomic level. The results shown that, firstly, high pressure decreased the intramolecular hydrogen bonds and increased the amylose-solvent hydrogen bonds, which is consistent with the process of high pressure starch gelatinization. Secondly, high pressure made amylose polymers more "stout". Meanwhile, high pressure decreased the angle of α-1,4 glycosidic linkage and increased the dihedral angles of α-1,4 glycosidic linkage, which indicates that pressure has obvious effects on amylose molecular conformation. Thirdly, high pressure made amylose polymers more stable. Moreover, in view of the results of energies, HHP may have an opposite gelatinization mechanism to heating. The results may be complementary to the existing experimental phenomena and provide theoretical guidance value for the using of HHP in starch processing.

1. Introduction

As one of the most abundant renewable resources in nature, starch plays a major role in food processing. The essence of processing starch is changing its external conditions, such as temperature, pressure, pH, ion concentration et cetera, to make the macroscopic properties meet the requirement of producers (Shujun & Copeland, 2015). HHP (high hydrostatic pressure) is one of the most important technologies in the field of food processing, which can effectively change the texture and extend the shelf life of food. Compared with traditional heating process, HHP's most distinct advantage is that it can more effectively avoid the degradation of pigments, the destruction of flavor substances and the loss of nutritional components (Yamamoto, 2017).

As shown in Fig. S1, in order to improve the efficiency of the using of HHP in starch processing, in recent years, by using rheometer, DSC (differential scanning calorimeter), RVA (rapid viscosity analyzer), TEM (Transmission electron microscopy), SEM (scanning electron microscopy), AFM (atomic force microscopy) XRD (X-ray diffraction) or NMR (nuclear magnetic resonance), numerous studies focused on the macroscopic properties, granule morphologies, crystalline properties and structural characteristics of starch have been done. At the macroscopic properties level, high pressure changes the thermostability, viscosity, retrogradation characteristics, alkaline water retention, water absorption capacity, oil absorption capacity, enzymatic hydrolysis efficiency and digestibility of starch (Yang et al., 2016; Hu, Zhang, Jin, Xu, & Chen, 2017; Liu, Wang, Cao, Fan, & Wang, 2016; Mu, Zhang, Raad, Sun, & Wang, 2015; Szwengiel, Lewandowicz, Górecki, & Błaszczak, 2017); at the micron-sized granule level, after high pressure treatments, the granule morphology of starch expands and adheres (Ahmed, Thomas, Taher, & Joseph, 2016), while holes and hollows appear as well (Huang, Jao, & Hsu, 2009); furthermore, at the atomic or molecular level, under high pressure, the transformation of starch crystals from A-type to B-type can be observed when using XRD (Yang, Gu, & Hemar, 2013; Yang et al., 2016), the reduction of starch molecular weight can be observed when using gel chromatography, (Szwengiel et al., 2017), and the changes of chemical shifts in the carbon atoms of starch molecule can be detected when using NMR (Sun, 2015).

* Corresponding author.
E-mail address: huangjunrongsxkjdx@126.com (H. Jun-rong).
[1] Co-first author.

https://doi.org/10.1016/j.foodchem.2020.127047
Received 15 October 2019; Received in revised form 7 May 2020; Accepted 11 May 2020
Available online 19 May 2020
0308-8146/

However, most of these studies are focus on the effects of HHP on the macroscopic properties, crystalline properties and granule morphological of starch at the micron-sized granules level, yet studies at the nanoscale atomic level are rarely performed. Namely, most research tried to explain the internal mechanism of the effects of HHP on starch characteristic from the micron-sized change at the granules level. For instance, after high pressure treatments were performed, a scanning electron microscope was used to observe the morphological properties of granules, and it was found that starch granules expanded and adhered, moreover, a rheometer was used to discover the viscosity value, and an increased viscosity was observed, therefore, the conclusion was drawn that an increase of viscosity is correlated closely with the adherence or expansion of starch granules (Ahmed et al., 2016; Huang et al., 2009). In another example, after high pressure treatments, a scanning electron microscope was used to observed the morphological properties of granules, and it was observed that holes and hollows appeared, concurrently, an enzymatic hydrolysis test was performed, which found an increase of enzymatic hydrolysis efficiency, lastly, the conclusion was reached that the increase of enzymatic hydrolysis efficiency is closely related to the presence of holes and hollows on the starch granules (Mu et al., 2015). Very few studies have tried to detail the internal mechanism of HHP's effects on starch characteristics at the atomic nanoscale level though (Sun, 2015), such as why high pressure results in particle expansion, why high pressure causes crystalline type conversions, et cetera.

The study of chemical structure at the atomic level or molecular conformation requires extremely delicate equipment such as NMR, AFM or GPC-MALLS (Gel permeation chromatography-multi-angle laser light scattering). However, because of their extremely high testing costs and tedious pretreatment, it leaves these methods with no obvious advantage over molecular simulation technology (Kumari, Sandhu, Ahmed, & Akhter, 2017). Moreover, Because of the high molecular weight of starch, in order to dissolve it completely when testing, a solution such as DMSO (dimethyl sulfoxide), but not water, is usually needed. However, it has been reported that the molecular conformation of starch in different proportions of water and DMSO have obvious differences (Tusch, Kruger, & Fels, 2011), and the common processing medium of starch is water, thus it may be difficult to detect the real conformation of starch.

Molecular dynamics simulation is essentially a scientific calculation method, which relies on Newtonian mechanics, and can calculate the motion state of each particle in a whole system by solving the kinematic equation in a very short time through various programs like Materials Studio, Gromacs, Amber, Discover et cetera. By analyzing the trajectory files, thermal properties, mechanical properties and structure information of models can be obtained (Kumari et al., 2017). Due to its high efficiency, low cost and multiple functions, molecular dynamics simulation has been widely used in material science (Rahimi, Amjad-Iranagh, & Modarress, 2016), biology (Huber, Marzinek, Holdbrook, & Bond, 2017) and the medical field (Appiah-Kubi, Olotu, & Soliman, 2019). Furthermore, In the area of carbohydrates, more and more studies about molecular dynamics simulation have emerged in recent years (Cheng et al., 2018; Winger, Christen, & Van Gunsteren, 2009; Tusch et al., 2011; Alvira, 2019).

In this study, molecular dynamics simulation was used to explore the effects of pressure on amylose molecular conformation at atomic level, which may be complementary to the existing experimental phenomena. The results of this study may provide theoretical guidance value for the using of HHP in starch processing.

2. Methods

Molecular dynamics simulation usually uses simple models to ensure efficient operation of the simulation. For example, Cheng et al., used a V-form helix with 26 residues as the initial model (Cheng et al., 2018), Winger and his associates used an amylose model with 9 residues as the initial model (Winger et al., 2009), While Tusch, Kruger and Fels used a V-form helix with 56 residues as the initial model (Tusch et al., 2011). Consequently, in this study, a V-form helix amylose model with 55 residues and a left-hand helix amylose model with 55 residues were used initially.

The pressure conditions for the present simulation were set at: 0.1 MPa, 1 MPa, 150 MPa, 300 MPa, 450 MPa, 600 MPa, 750 MPa, 900 MPa, with three parallel simulations of each pressure. Berendsen barostat and Langevin were chosen to control the pressure and temperature (300 K) conditions respectively. Every simulation was carried out using the Amber 2018 program, with glycam 06 and tip5p force fields in the NPT (number of particles, pressure and temperature) ensemble for 100 ns, after the equilibrium of 2 ns in the NVT (number of particles, volume and temperature) ensemble. Further, a leap-frog scheme, periodic boundary conditions and an appropriate 1 nm cutoff distance was used.

Simulation files were extracted every 0.01 ns to calculate the numbers of hydrogen bonds, angles, atomic distances, SASA (solvent accessible surface area), Rg (radius of gyration), RMSF (root mean square fluctuation), RMSD (root mean square deviations), energies and pyranose ring conformation distributions. The atomic distances, angles, dihedral angles, SASA and Rg were calculated to evaluate the changes of molecular conformation. The energies, RMSD, RMSF and pyranose ring conformation were calculated to evaluate the stability of amylose molecular conformation. Moreover, in each pressure gradient, the average value of RMSF, RMSD, angles and distances were calculated using all the residues of each conformation in every parallel simulation. The presence of a hydrogen bond was determined by the criteria in which the maximum distance between the donor and acceptor atoms is 0.35 nm. The pyranose ring conformation was calculated by using Cremer–Pople coordinates. The SASA was calculated by using LCPO (linear combination of pairwise overlaps) algorithm of Weiser definition.

3. Results and discussion

In the whole simulation processes (see the Supplementary videos), slight bending of both the V-form helix and left-hand helix could be observed in any pressure gradient. It should be noted that, because there is only one visual angle of the videos, so it may be difficult to distinguish between bending and twining sometimes (actually, according the results of SASA below, there was no twining during the simulations). Besides, because of the more compact initial structure of V-form helix, it seems exhibited higher bending degree than left-hand helix. However, the V-form helix gradually degraded in the first few nanometers, then, they exhibited no obvious differences of the angles, distances or pyranose ring conformations etc. (see below)

Furthermore, the hydrogen bonds was marked in red in the Supplementary videos, however, it is difficult to distinguish the differences between different pressure gradients. Therefore, a table was used to clearly exhibited the effects of HHP on the hydrogen bonds of amylose polymers. (see below)

3.1. Hydrogen bonds

Hydrogen bonds involve a special intermolecular, or intramolecular interaction, which are not as strong as covalent bonds but are more stable than electrostatic and VDW (Van der Waals) interactions. On the one hand, since hydrogen bonds are more stable than electrostatic and VDW interactions, they are extremely significant in maintaining the structure of starch. On the other hand, it is much easier to destroy the hydrogen bonds compared to the covalent bonds during processing, specifically because the hydrogen bonds are more unstable during processing. Therefore, this makes hydrogen bonds a key factor in changing some macroscopic properties, including starch structure, during processing. Generally, hydrogen bonds are formed by an

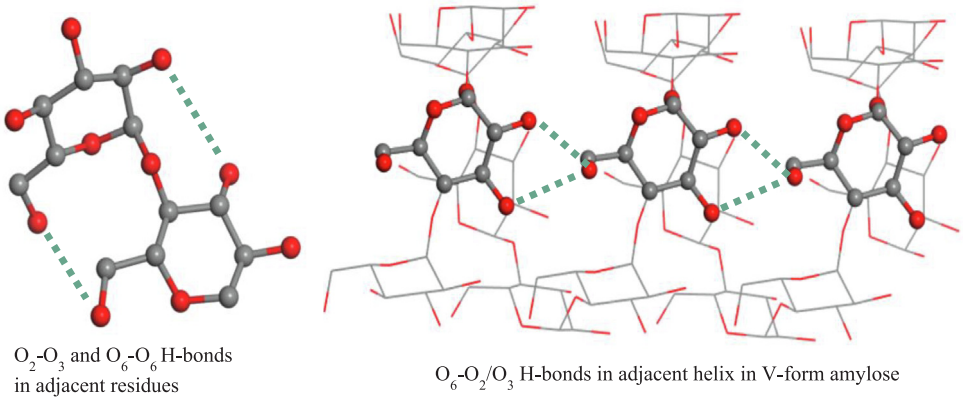

Fig. 1. Different hydrogen bonds in amylose (Chen, Huang, Pu, Fang, & Yang, 2020).

interaction between the lone pair electrons from an electronegative acceptor atom and the polar donor-H bond's hydrogen atom. An acceptor and donor can come from the same atom, but the size of the atomic radius must be small (as in elements like O, N or F.), the distance between the acceptor and donor must be below 0.35 nm while the maximum angle of the donor-H-acceptor is 60°. Starch glucose residues have an abundance of hydroxyls that just satisfy the conditions for hydrogen bond formation.

3.1.1. Intramolecular hydrogen bonds

O_2-O_3 and O_6-O_6 intramolecular hydrogen bonds are commonly formed by two neighboring glucose residues (Fig. 1). As shown in Table 1a, O2-O3 and O6-O6 intramolecular hydrogen bonds of both the V-form helix and left-hand helix decreased with increasing pressure levels. However, O_6-O_6 intramolecular hydrogen bonds were less affected by pressure. O_6-O_2/O_3 intramolecular hydrogen bonds, which is suited between neighboring turns of the helix, play an important role for maintaining structure of V-form helix (Fig. 1). In the V-form helix, with the increase of pressure, the number of O_6-O_2/O_3 hydrogen bonds decreased quickly in the first 4 ns. When pressure reached 450 MPa, the number of hydrogen bonds dropped to 0. It appears that high pressure will accelerate the degradation of a V-form helix. This is in accordance with Tusch and Cheng's results (Tusch et al., 2011; Cheng et al., 2018), which demonstrated that the hydrogen bond numbering between O_6 and O_2/O_3 decreased to 0 at around 4.5 ns when the amylose polymers were in the presence of water (Tusch et al., 2011). Furthermore, no O_6-O_2/O_3 hydrogen bond could be observed in the left-hand helix.

3.1.2. Amylose-solution hydrogen bonds

On the other hand, in both the V-form helix and left-hand helix, the hydrogen bonds formed by amylose and water increased gradually with increasing pressure levels. As acceptors, the hydrogen bond numbers of O_2, O_3, O_5 and O_6 increased at different degrees (Table 1b). As donors, it did not matter whether the donors were O2, O3 or O6, the number of solvent-amylose hydrogen bonds were less affected by the change of pressure. In other words, at high pressure, the hydroxyls on amylose more prefer being H donors, but not H acceptors, to form more hydrogen bonds with solvents. Furthermore, high pressure also affects the water hydrogen bond network, which has been proven by early studies (Lin, Kai, & Zi, 2015), so there are dual effects on solvent-amylose hydrogen bonds under pressure.

Moreover, under certain conditions of starch gelatinization, water molecules penetrate starch granules which create new hydrogen bonds with the starch molecules. During this process, intramolecular hydrogen bonds are destroyed and alter the original structure (Stolt, Oinonen, & Autio, 2001). Our results have shown that high pressure decreased intramolecular bonds, yet amplified the molecule-solvent hydrogen bonds, and these findings are accordance to existing high pressure starch gelatinization experimental phenomena.

3.2. Molecular conformation

The atomic distances, angles, dihedral angles, SASA and Rg were calculated to evaluate the changes of amylose molecular conformation under different pressure.

3.2.1. Atomic distances

The distances of atoms can directly signify the change of molecular conformation in amylose polymers. As shown in Fig. 2a, d and g, the 6 residue distances of both the V-form helix and left-hand helix gradually decreased with the increase of pressure. It appears that high pressure will make amylose polymers become more "stout". As shown in Fig. 2b and e, no effects of pressure on the O_3-$C5_{n+3}$ distance of left-hand helix could be observed. It seems that the O_3-$C5_{n+3}$ distance of the V-form helix approximately increased with the rise of pressure. According to the result of O_2/O_3-O_6, high pressure will accelerate the degradation of the V-form helix. As the internal diameter of the V-form helix, the O_3-$C5_{n+3}$ distance of the V-form helix is much lower than the O_3-$C5_{n+3}$

Table 1a
The numbers intramolecular hydrogen bond of V-form helix and left-hand helix.

V-form	0.1 MPa	1 MPa	150 MPa	300 MPa	450 MPa	600 MPa	750 MPa	900 MPa
O_2-O_3	21.67 ± 0.94^{Aa}	19.67 ± 0.47^{Ab}	16.67 ± 2.45^{Ab}	11.33 ± 2.05^{Ab}	9.67 ± 1.25^{Ab}	7.67 ± 0.47^{Ab}	4.33 ± 1.71^{Bc}	1.67 ± 2.50^{Bc}
O_6-O_6	41.67 ± 3.29^{Aa}	44.67 ± 4.18^{Aa}	39 ± 1.63^{Aa}	40.33 ± 2.86^{Aa}	38.67 ± 4.49^{Aa}	36.67 ± 1.71^{Aa}	33.67 ± 0.82^{Bb}	31.33 ± 3.29^{Bb}
O_6-O_2/O_3 1–4 ns	10.67 ± 2.05^{Aa}	4.67 ± 0.82^{Bb}	1.33 ± 0.47^{Cc}	0.33 ± 0.47^{Cc}	0^{Cc}	0^{Cc}	0^{Cc}	0^{Cc}
O_6-O_2/O_3 4–100 ns	0^{Aa}	0^{Aa}	0^{Aa}	0^{Aa}	0^{Aa}	0^{Aa}	0^{Aa}	0^{Aa}
Left-hand	0.1 MPa	1 MPa	150 MPa	300 MPa	450 MPa	600 MPa	750 MPa	900 MPa
O_2-O_3	18.67 ± 1.25^{Aa}	16.33 ± 1.71^{Aa}	15 ± 0.81^{Aa}	11.33 ± 2.62^{Ab}	9.67 ± 2.50^{Ab}	7 ± 0.81^{Ab}	4.33 ± 1.71^{Ac}	1.33 ± 0.47^{Ad}
O_6-O_6	38.67 ± 2.05^{Aa}	37.33 ± 2.86^{Aa}	35.33 ± 2.16^{Aa}	32.67 ± 3.29^{Aa}	33.33 ± 0.47^{Aa}	30.67 ± 1.63^{Ab}	28.33 ± 0.47^{Ac}	25 ± 1.63^{Bd}
O_6-O_2/O_3 1–4 ns	0^{Aa}	0^{Aa}	0^{Aa}	0^{Aa}	0^{Aa}	0^{Aa}	0^{Aa}	0^{Aa}
O_6-O_2/O_3 4–100 ns	0^{Aa}	0^{Aa}	0^{Aa}	0^{Aa}	0^{Aa}	0^{Aa}	0^{Aa}	0^{Aa}

*Different capital letters in different pressures: $P < 0.01$; different lowercase letters in different pressures: $P < 0.05$.

Table 1b
The numbers of solvent-amylose hydrogen bond of V-form helix and left-hand helix.

V-form	Acceptor O_2	Acceptor O_3	Acceptor O_6	Acceptor O_5	Donor O_2	Donor O_3	Donor O_6	Total
0.1 Mpa	31.33 ± 2.45^{Aa}	17.67 ± 2.86^{Aa}	20.67 ± 1.25^{Aa}	5.33 ± 1.71^{Aa}	38.33 ± 0.81^{Aa}	44.67 ± 1.41^{Aa}	41.67 ± 0.47^{Aa}	199.67 ± 4.32^{Aa}
1 Mpa	29.67 ± 1.41^{Aa}	18.33 ± 0.81^{Aa}	21 ± 1.63^{Aa}	7.33 ± 0.47^{Aa}	40.67 ± 2.44^{Aa}	44.33 ± 0.81^{Aa}	42.67 ± 3.26^{Aa}	204 ± 4.64^{Aa}
150 Mpa	34.67 ± 0.81^{Ab}	21 ± 2.16^{Aa}	26.33 ± 1.51^{Ab}	8.67 ± 0.47^{Aa}	45.33 ± 3.55^{Aa}	46.33 ± 3.30^{Aa}	46 ± 2.87^{Aa}	228 ± 8.37^{Bb}
300 Mpa	35 ± 1.87^{Ab}	21.67 ± 0.76^{Aa}	28.67 ± 1.71^{Ab}	8 ± 0.82^{Aa}	42.67 ± 1.69^{Aa}	44.67 ± 4.49^{Aa}	46.33 ± 3.68^{Aa}	227 ± 7.41^{Bb}
450 Mpa	40.67 ± 3.40^{Ab}	21.33 ± 2.16^{Aa}	29 ± 1.63^{Ab}	13.33 ± 1.24^{Bb}	41.33 ± 2.87^{Aa}	43.33 ± 3.27^{Aa}	43 ± 2.16^{Aa}	232 ± 7.78^{Bb}
600 Mpa	42.33 ± 1.25^{Ab}	33.67 ± 3.68^{Bb}	35 ± 2.87^{Bc}	14.67 ± 0.94^{Bb}	47.67 ± 1.63^{Ab}	48 ± 1.41^{Aa}	48.33 ± 2.05^{Aa}	269.67 ± 4.89^{Cc}
750 Mpa	48.67 ± 2.49^{Bc}	37.67 ± 1.63^{Bb}	42.33 ± 1.25^{Cd}	21.33 ± 1.71^{Cc}	50.33 ± 2.05^{Ab}	47.33 ± 0.47^{Aa}	49.67 ± 1.25^{Aa}	297.33 ± 4.49^{Dd}
900 Mpa	50.33 ± 1.41^{Bc}	42.67 ± 0.81^{Cc}	45.33 ± 1.63^{Cd}	29.67 ± 1.41^{Dd}	49 ± 1.25^{Ab}	54.67 ± 1.71^{Bb}	51.33 ± 2.49^{Aa}	323 ± 5.71^{Ee}
Left-hand	Acceptor O_2	Acceptor O_3	Acceptor O_6	Acceptor O_5	Donor O_2	Donor O_3	Donor O_6	Total
0.1 Mpa	34.33 ± 2.86	19.67 ± 2.45^{Aa}	23.33 ± 1.71^{Aa}	5.67 ± 0.81^{Aa}	43.33 ± 2.16^{Aa}	48 ± 3.26^{Aa}	49.67 ± 1.25^{Aa}	224 ± 4.18^{Aa}
1 Mpa	34 ± 3.26^{Aa}	20.33 ± 2.62^{Aa}	22.67 ± 0.82^{Aa}	8.67 ± 0.94^{Bb}	42.67 ± 2.62^{Aa}	46.33 ± 2.94^{Aa}	46.33 ± 3.74^{Aa}	221 ± 8.16^{Aa}
150 Mpa	36.67 ± 1.71^{Aa}	22 ± 2.16^{Aa}	25.67 ± 1.89^{Ab}	9.67 ± 0.47^{Bb}	44.33 ± 0.82^{Aa}	48.67 ± 1.25^{Aa}	45.33 ± 2.89^{Aa}	232.33 ± 6.59^{Aa}
300 Mpa	38.33 ± 1.63^{Aa}	26 ± 1.41^{Ab}	25.33 ± 3.55^{Ab}	11.67 ± 0.81^{Bc}	43 ± 3.68^{Aa}	50.33 ± 2.87^{Aa}	46.67 ± 1.63^{Aa}	241.33 ± 5.35^{Aa}
450 Mpa	42.67 ± 1.25^{Ab}	27.33 ± 0.81^{Ab}	28.33 ± 0.94^{Ab}	14.33 ± 2.49^{Bc}	45.67 ± 0.81^{Aa}	51 ± 1.41^{Aa}	49 ± 0.82^{Aa}	258.33 ± 5.31^{Bb}
600 Mpa	44.67 ± 1.25^{Ab}	33.33 ± 2.16^{Bc}	34.67 ± 2.86^{Bc}	16 ± 0.81^{Bc}	49.67 ± 3.29^{Aa}	52.33 ± 2.45^{Aa}	50.33 ± 3.74^{Aa}	281 ± 5.73^{Cc}
750 Mpa	46.67 ± 2.86^{Ab}	41 ± 0.81^{Cd}	40.67 ± 2.16^{Bd}	24.67 ± 2.94^{Cd}	48.67 ± 1.25^{Aa}	50.33 ± 1.63^{Aa}	52.33 ± 2.45^{Aa}	304.33 ± 6.94^{Dd}
900 Mpa	50.33 ± 2.05^{Ab}	48.67 ± 3.74^{De}	47.33 ± 2.49^{Ce}	32.33 ± 1.41^{De}	54.67 ± 0.94^{Bb}	56 ± 0.82^{Bb}	55.67 ± 4.18^{Aa}	345 ± 7.84^{Ee}

*Different capital letters in different pressures: $P < 0.01$; different lowercase letters in different pressures: $P < 0.05$.

distance of the degraded V-form helix. Although the V-form helix will degrade in the first few nanoseconds, only subtle differences were still observed. Therefore, there may be a relationship between the degradation rate of the V-form helix and the approximate increase of O_3-$C_{5\ n+3}$ distance.

The end-to-end distances were detected in order to observe the bending, folding or twining of amylose polymers. The low end-to-end distances may indicate the high degree of the bending, folding or twining of amylose polymers. However, no obvious trends of end-to-end distances of both the V-form helix and the left-hand helix were observed with the changes of pressure (Fig. 2c and 2f). This may be due to the large random fluctuation of the two flexible heads, which was evinced by the results of RMSF (see below). Furthermore, the end-to-end distance of the fully extended left-hand helix model or the degraded V-form helix model is about 21 nm. However, the end-to-end distances of both the V-form helix and left-hand helix in all pressures were about 12 nm to 16 nm. Thus, slight bending of both the left-hand helix and the V-form helix occurred in the simulations.

3.2.2. Angles and dihedral angles of α-1,4 glycosidic linkage

Previous research has shown that the angle and dihedral angles of α-1,4 glycosidic linkage are extremely significant with regard to the change of amylose molecular conformation (Gidley & Bociek, 1985). These past experiments demonstrated that the C_1 and C_4 glycosidic sites were more responsive to conformational changes when compared to the C_2, C_3, and C_5 carbons. This is because the C_1 and C_4 carbons showed greater dispersions of chemical shift under the various conformations of the α-1,4 glycosidic linkage. As seen in Fig. 3a–f, in the both V-form helix and the left-hand helix, angle C_1-O_4'-C_4 gradually decreased, dihedral angle C_1-O_4'-C_4'-C_5' and O_5-C_1-O_4'-C_4' gradually increased with the increase of pressure.

However, high pressure may not only affect the α-1,4 glycosidic linkage, but also all the angles or bonds in amylose polymers (Sun, 2015). In order to verify whether the angle and dihedral angles of the α-1,4 glycosidic linkage have significant effects on amylose molecular conformation, models with specified angles or dihedral angles were built to exhibit their effects on molecular conformation by using Gaussview 5.09. As shown in Fig. 3g, the results indicate that, with the decrease of angle C_1-O_4'-C_4' and increase of dihedral angle C_1-O_4'-C_4'-C_5' and O_5-C_1-O_4'-C_4', the 6 residue distances gradually decreased, which is in accordance with the previous results. Therefore, the angle and dihedral angles of the α-1,4 glycosidic linkage do have great significance for the change of amylose molecular conformation.

3.2.3. Solvent accessible surface area

The SASA of the V-form helix and left-hand helix were detected in order to further observe the bending, folding and twining of amylose polymers. The low SASA may indicate a high degree of folding or twining in the amylose polymers. As shown in Fig. 4a and c, with the increase of pressure, the total SASA of both the V-form and left-hand helix gradually decreased. However, there were no valleys of SASA values in Fig. 4b and 4d, all the residues' SASA were above 1 nm^2 (The average residue SASA of double-amylose model is about 0.7 nm^2), which indicated that no obvious folding or twining of amylose polymers appeared in any pressure gradient. Therefore, with the increase of pressure, the small reduction of SASA in the amylose polymers may be related to the decrease of 6 residue distances.

3.2.4. Rg

The distance between every atom and the center of the molecule is denoted by the Rg, so a smaller Rg means the structure is more compact. In Fig. S2, no obvious trend of the Rg in both the V-form helix and left-hand helix were observed during the change of pressure. Considering that high pressure decreased the distances of 6 residues, but had no effects on Rg, this may indicate that high pressure will make amylose polymers be more "stout", yet not "shorter". Furthermore, it also could be that Rg may not be a sufficiently accurate index for linear molecules due to the two flexible heads, which makes the small differences of Rg difficult to detect.

3.3. Stability of molecular conformation

The energies, RMSD, RMSF and pyranose ring conformation of amylose polymers were calculated to evaluate the stability of amylose molecular conformation.

3.3.1. Energies

The bond stretching, angle bending, dihedral angle torsion, VDW (Van der Waals) and electrostatic energies can indicate the stability of amylose. The lower these energies are, the more stable the amylose polymers will be. In Fig. S3, in both the V-form helix and the left-hand helix, with the increase of pressure, the bond stretching, angle bending, electrostatic and total energies gradually decreased, however, VDW energies increased gradually. No effects of pressure on dihedral angle torsion energies was observed though. From the above results, one can see that high pressure decreased the total energies of both the V-form and left-hand helix, making the amylose polymers more stable, which is in accordance with Orlowska's research (Orlowska, Utzig, & Randzio,

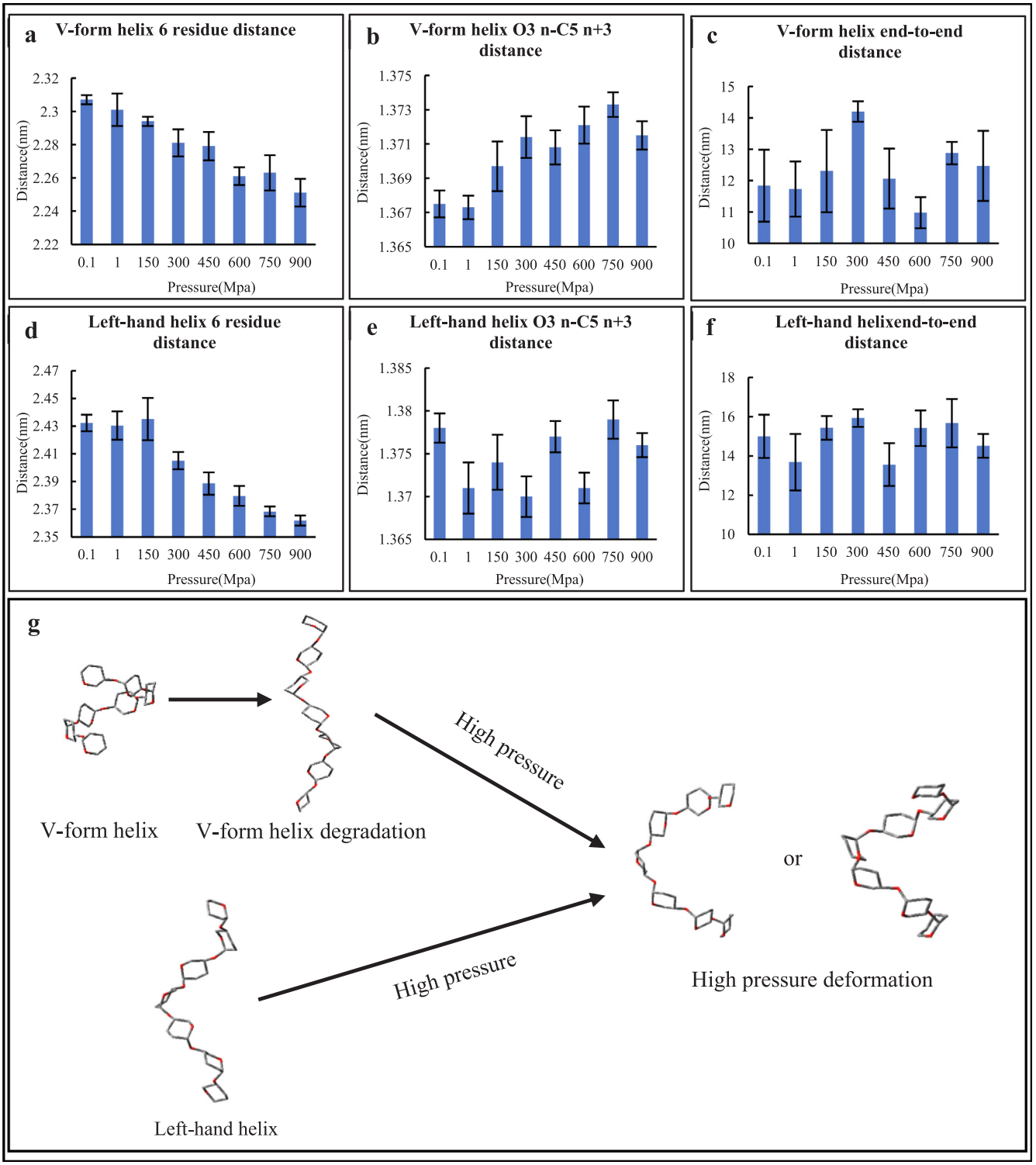

Fig. 2. The distances of 6 residues (a, d), O_3-$C_{5\ n+3}$ (b, e) and end-to-end (c, f) of the V-form helix and left-hand helix in different pressures.

2010).

In the early years, several researchers suggested that heat and high pressure operate similarly when it comes to starch gelatinization. For one, higher pressure and heating both start by hydrating the amorphous region, then the granules expand, and finally the crystalline region is destroyed (Rubens, Snauwaert, & Heremans, 1999). Thereafter, this theory was confirmed by other researchers using laser-scanning confocal microscopy and scanning electron microscopes to observe the gelatinization process caused by heating and high pressure respectively (Katleen, Vallons, & Arendt, 2009). However, this theory was also questioned by a minority of researchers, because they discovered that high pressure gelatinization caused a smaller degree of expansion in starch granules compared to heating gelatinization during the gelatinization process (Stolt et al., 2001). In order to verify whether the heating gelatinization mechanism is the same as the high pressure mechanism, three simulations in the same pressure, but different temperatures (4℃, 50℃, 100℃), were carried out. The results showed that heating will increase the energies of amylose polymers.

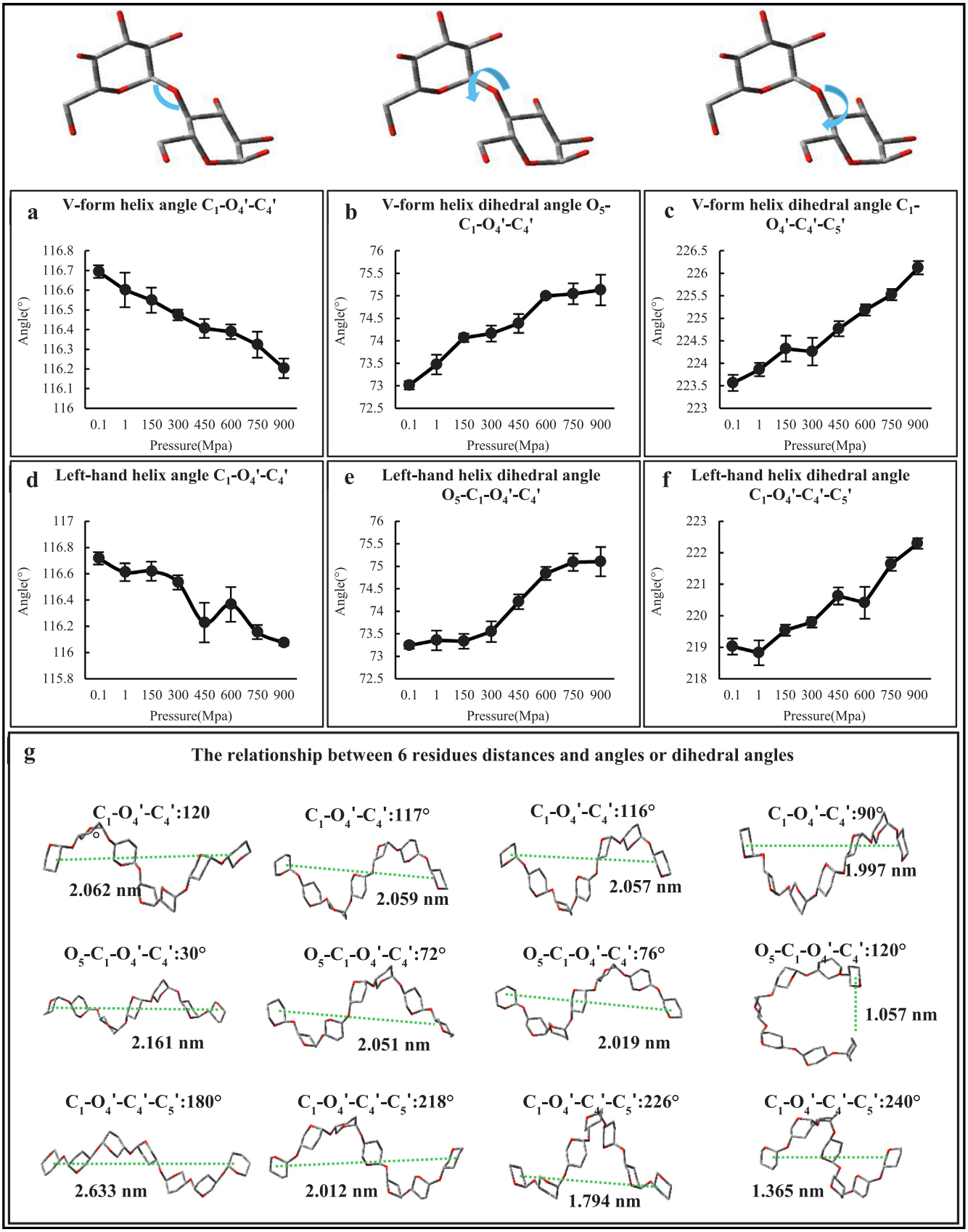

Fig. 3. The angle C_1-O_4′-C_4′ (a, d), dihedral angle O_5-C_1-O_4′-C_4′ (b, e) and C_1-O_4′-C_4′-C_5′ (d, f) of the V-form helix and left-hand helix in different pressures. g: the relationship between 6 residues distances and angles or dihedral angles.

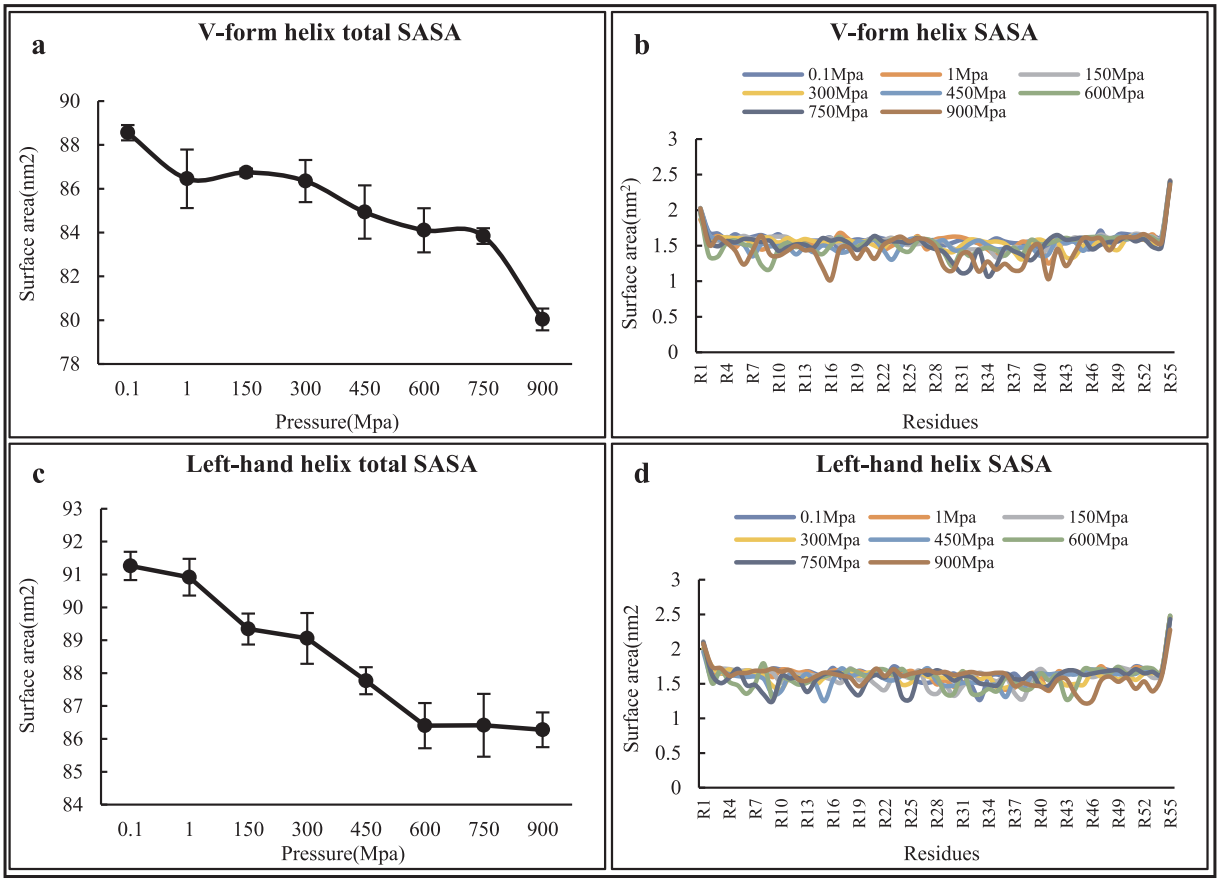

Fig. 4. The total SASA (a, c) and residues' SASA (b, d) of the V-form helix and left-hand helix in different pressures.

Thus, even though the processes of both high pressure and heating begin by hydrating the amorphous region, causing the granules to expand, which leads to the crystalline region being destroyed (Rubens et al., 1999). However, with respect to energy, the high pressure and heating mechanisms are complete opposites, specifically, the high pressure and heating hydration mechanisms may be different.

3.3.2. RMSD and RMSF

The RMSD signifies the relative amylose molecular conformation deviations during different periods of the simulation, while the RMSF indicates the fluctuation patterns of every amylose residue. As seen in Fig. S4, for both amylose models, the average RMSF values of all the residues and the RMSD values both gradually decreased with the increase of pressure. It appears that high pressure will decrease the fluctuation range of amylose polymers, which is in accordance with the results of studying the energies mentioned above and Orlowska's research (Orlowska et al., 2010).

Moreover, both amylose models showed, at any pressure, that the two heads had higher RMSF values than the other parts of the amylose polymers (Fig. S4c and S4f), indicating that the two head residues are more flexible than other amylose residues, which is in accordance with Cheng's results (Cheng et al., 2018).

3.3.3. Pyranose ring conformation

Glucose residues in starch molecules are frequently in a 4C1 chair state (Iben, Søren, Andreas, Birger, & Mohammed, 2010), the most stable conformation which uses the smallest amount of binding free energy (Fig. S5a) (Chen et al., 2020; Anthony & Peter, 2007; Sega, Autieri, & Pederiva, 2011). That being said, the glucose residues' conformations may convert to 1C4 chair, half-chair, boat, skew-boat, or other conformations when external environmental conditions affect the molecules. Therefore, a puckering analysis was conducted, using Crème-Pople coordinates (Cremer & Pople, 1975), in order to analyze the effects of pressure on the residues' conformation. When θ values are above 135°, a chair 1C4 conformation is created, but if θ is somewhere between 0° and 45° the residues present a chair 4C1 conformation, moreover, the residues form other conformations when θ is between 45° and 135° (Sega et al., 2011).

As Fig. S5b and S5c show, with the increase of pressure, the content of 4C1 chair conformations of both the V-form helix and the left-hand helix gradually increased. This indicates that high pressure makes starch molecules become more stable, which is in accordance with the results found when analyzing the energies, RMSD and RMSF above.

4. Conclusions

In this study, molecular dynamics simulation was used to explore the effects of pressure on amylose molecular conformation at the atomic level. The results show that, firstly, high pressure decreased the intramolecular hydrogen bonds, and increased the amylose-solvent hydrogen bonds, which is consistent with the process of high pressure starch gelatinization. Secondly, high pressure made amylose polymers more "stout". Meanwhile, high pressure decreased the angle of α-1,4 glycosidic linkage and increased the dihedral angles of α-1,4 glycosidic linkage, which indicates that pressure has obvious effects on amylose molecular conformation. Thirdly, high pressure made the amylose polymers more stable, which was proven by the analyses of energies, RMSD, RMSF and pyranose ring conformation. Moreover, in view of the results of energies, we speculated that high pressure gelatinization and heating gelatinization may operate under opposite mechanisms.

In recent years, in order to improve the efficiency of the using of HHP in starch processing, an abundance of studies about the effects of

HHP on the macroscopic properties, granule morphologies, crystalline properties and structural characteristics of starch have been done (Fig. S1). Nonetheless, it is still difficult to fully explain how nanoscale change at the atomic level, micron-sized change at the level of the granule and the visual change of macroscopic properties relate to each other. Because different characterization methods have different pointcuts and the microcosmic structure of starch granules is still controversial at present (French, 1972; Bertoft, 2013; Bertoft, 2017). This study may be complementary to existing experimental phenomena though.

Hopefully, if the structure of starch is fully understood sometime in the near future, the findings could serve as a significant reference for explaining the relationships among the nanoscale change at the level of the atom, the micron-sized changes at the level of the granule, and the visual alteration of macroscopic properties.

Author contributions

Chen Zhi-guang and Huang Jun-rong contributed significantly to analysis and manuscript preparation; Shu Guo-wei contacted other computing centers that were still running; Zhang Hong-hui helped us finish the supplementary simulations; Wade Keipper helped proofread the manuscript; Pu Hua-yin helped perform the analysis with constructive discussions; Yang Qi and Fang Chen-lu performed the data analyses and wrote the manuscript.

Declaration of Competing Interest

The authors declare that they have no known competing financial interests or personal relationships that could have appeared to influence the work reported in this paper.

Acknowledgements

This work is supported by the National Natural Science Foundation of China (Code: 31772012).

Appendix A. Supplementary data

Supplementary data to this article can be found online at https://doi.org/10.1016/j.foodchem.2020.127047.

References

Ahmed, J., Thomas, L., Taher, A., & Joseph, A. (2016). Impact of high pressure treatment on functional, rheological, pasting, and structural properties of lentil starch dispersions. *Carbohydrate Polymers, 152*, 639–647. https://doi.org/10.1016/j.carbpol.2016.07.008.

Alvira, E. (2019). Molecular simulation of the separation of isoleucine enantiomers by β-cyclodextrin. *Molecules, 24*(6), 14–19. https://doi.org/10.3390/molecules24061021.

Anthony, D. H., & Peter, J. R. (2007). Puckering coordinates of monocyclic rings by triangular decomposition. *Journal of Chemical Information and Modeling, 47*, 1031–1035. https://doi.org/10.1021/ci600492e.

Appiah-Kubi, P., Olotu, F. A., & Soliman, M. (2019). Probing binding landscapes and molecular recognition mechanisms of atypical antipsychotic drugs towards the selective targeting of D_2 dopamine receptor. *Molecular Informatics*. https://doi.org/10.1002/minf.201900044. (Online published).

Bertoft, E. (2013). On the building block and backbone concepts of amylopectin structure. *Cereal Chemistry, 90*, 294–311.

Bertoft, E. (2017). Understanding starch structure: Recent progress. *Agronomy, 7*, 55–56. https://doi.org/10.3390/agronomy7030056.

Chen, Z. G., Huang, J. R., Pu, H. Y., Fang, C. L., & Yang, Q. (2020). The Effects of HHP (High Hydrostatic Pressure) on the Interchain Interaction and the Conformation of Amylopectin and Double-amylose Molecules. *International Journal of Biological Macromolecules, 155*, 91–102. https://doi.org/10.1016/j.ijbiomac.2020.03.190.

Cheng, L., Tao, F., Boyu, Z., Xiao, Z., Bruce, H., Hui, Z., & Osvaldo, C. (2018). A molecular dynamics simulation study on the conformational stability of amylose-linoleic acid complex in water. *Carbohydrate Polymers, 196*, 56–65. https://doi.org/10.1016/j.carbpol.2018.04.102.

Cremer, D., & Pople, J. A. (1975). A general definition of ring puckering coordinates. *Journal of the American Chemical Society, 6*(97), 1354–1358.

French, D. (1972). Fine structure of starch and its relationship to the organization of starch granules. *Journal of Japan Society Starch Science, 19*, 8–25.

Gidley, M. J., & Bociek, S. M. (1985). Molecular organization in starches: A 13C CP/MAS NMR study. *Journal of the American Chemical Society, 107*, 7040–7044.

Hu, X. P., Zhang, B., Jin, Z. Y., Xu, X. M., & Chen, H. Q. (2017). Effect of high hydrostatic pressure and retrogradation treatments on structural and physicochemical properties of waxy wheat starch. *Food Chemistry, 1*(232), 560–565. https://doi.org/10.1016/j.foodchem.2017.04.040.

Huang, S. L., Jao, C. L., & Hsu, K. C. (2009). Effects of hydrostatic pressure/heat combinations on water uptake and gelatinization characteristics of japonica rice grains: A kinetic study. *Journal of Food Science, 74*(8), 442–448. https://doi.org/10.1111/j.1750-3841.2009.01329.x.

Huber, R. G., Marzinek, J. K., Holdbrook, D. A., & Bond, P. J. (2017). Multiscale molecular dynamics simulation approaches to the structure and dynamics of viruses. *Progress in Biophysics and Molecular Biology, 128*, 121–132. https://doi.org/10.1016/j.pbiomolbio.2016.09.010.

Iben, D., Søren, B. E., Andreas, B., Birger, L. M., & Mohammed, S. M. (2010). First principles insight into the α-glucan structures of starch: Their synthesis, conformation, and hydration. *Chemical Reviews, 110*, 2049–2080. https://doi.org/10.1021/cr900227t.

Katleen, J., Vallons, E., & Arendt, K. (2009). Effects of high pressure and temperature on the structural and rheological properties of sorghum starch. *Food Science Emergency Technology, 10*, 449–456.

Kumari, I., Sandhu, P., Ahmed, M., & Akhter, Y. (2017). Molecular dynamics simulations, challenges and opportunities: A biologist's prospective. *Current Protein and Peptide Science, 18*(11), 1163–1179. https://doi.org/10.2174/1389203718666170622074741.

Lin, Z., Kai, M., & Zi, Y. (2015). Changes of water hydrogen bond network with different externalities. *International Journal of Molecular Sciences, 16*, 8454–8489. https://doi.org/10.3390/ijms16048454.

Liu, H., Wang, L., Cao, R., Fan, H., & Wang, M. (2016). In vitro digestibility and changes in physicochemical and structural properties of common buckwheat starch affected by high hydrostatic pressure. *Carbohydrate Polymers, 144*, 1–8. https://doi.org/10.1016/j.carbpol.2016.02.028.

Mu, T. H., Zhang, M., Raad, L., Sun, H. N., & Wang, C. (2015). Effect of α-amylase degradation on physicochemical properties of pre-high hydrostatic pressure-treated potato starch. *PLoS One, 10*(12), 14–20. https://doi.org/10.1371/journal.pone.0143620.

Orlowska, M., Utzig, E., & Randzio, S. L. (2010). Thermogravimetric study of water state in wheat starch gels obtained under high pressures. *Annals of the New York Academy of Sciences, 11*(89), 55–61. https://doi.org/10.1111/j.1749-6632.2009.05200.x.

Rahimi, A., Amjad-Iranagh, S., & Modarress, H. (2016). Molecular dynamics simulation of coarse-grained poly(L-lysine) dendrimers. *Journal of Molecular Modeling, 22*(3), 59. https://doi.org/10.1007/s00894-016-2925-0.

Rubens, P., Snauwaert, J., & Heremans, K. (1999). In situ observation of pressure-induced gelation of starches studied with FTIR in the diamond anvil cell. *Carbohydrate Polymers, 39*(3), 231–235.

Sega, M., Autieri, E., & Pederiva, F. (2011). Pickett angles and Cremer-Pople coordinates as collective variables for the enhanced sampling of six-membered ring conformations. *Molecular Physics, 1*(109), 141–148. https://doi.org/10.1080/00268976.2010.522208.

Shujun, W., & Copeland, L. (2015). Effect of acid hydrolysis on starch structure and functionality: A review. *Food Science and Nutrition, 55*(8), 1081–1097. https://doi.org/10.1080/10408398.2012.684551.

Stolt, M., Oinonen, S., & Autio, K. (2001). Effect of high pressure on the physical properties of barley starch. *Innovative Food Science and Emerging Technologies, 1*, 167–175.

Sun, P. R. (2015). *The effects of HHP on the structure of corn starch granules. Doctoral dissertation.* Beijing: China Agricultural University.

Szwengiel, A., Lewandowicz, G., Górecki, A. R., & Błaszczak, W. (2017). The effect of high hydrostatic pressure treatment on the molecular structure of starches with different amylose content. *Food Chemistry, 1*(240), 51–58. https://doi.org/10.1016/j.foodchem.2017.07.082.

Tusch, M., Kruger, J., & Fels, G. (2011). Structural stability of V-amylose helices in water-DMSO mixtures analyzed by molecular dynamics. *Journal of Chemical Theory and Computation, 7*(9), 2919–2928.

Winger, M., Christen, M., & Van Gunsteren, W. F. (2009). On the conformational properties of amylose and cellulose oligomers in solution. *International Journal of Carbohydrate Chemistry. International Journal of Carbohydrate Chemistry, 1*(9), 1–8. https://doi.org/10.1155/2009/307695.

Yamamoto, K. (2017). Food processing by high hydrostatic pressure. *Bioscience Biotechnology and Biochemistry, 81*(4), 1–8. https://doi.org/10.1080/09168451.2017.1281723.

Yang, Z., Gu, Q., & Hemar, Y. (2013). In situ study of maize starch gelatinization under ultra-high hydrostatic pressure using X-ray diffraction. *Carbohydrate Polymers, 97*(1), 235–238. https://doi.org/10.1016/j.carbpol.2013.04.075.

Yang, Z., Swedlund, P., Hemar, Y., Mo, G., Wei, Y., Li, Z., & Wu, Z. (2016). Effect of high hydrostatic pressure on the supramolecular structure of corn starch with different amylose contents. *International Journal of Biological Macromolecules, 85*, 604–614. https://doi.org/10.1016/j.ijbiomac.2016.01.018.